Dynamics for the Cl+C$_2$H$_6$→HCl+C$_2$H$_5$ reaction examined through state-specific angular distributions

S. Alex Kandel, T. Peter Rakitzis, Topaz Lev-On, and Richard N. Zare
*Department of Chemistry, Stanford University, Stanford, California 94305*

Photolysis of Cl$_2$ initiates the title reaction at a sharply defined collision energy of 0.24±0.03 eV. Nascent product rotational state distributions for HCl ($v=0$) are determined using resonance enhanced multiphoton ionization (REMPI), center-of-mass scattering distributions are measured by the core-extraction technique, and the average internal energy of the C$_2$H$_5$ product is deduced from the dependence of the core-extracted signal on the photolysis polarization. The HCl product has little rotational excitation, but the scattering distribution is nearly isotropic. Although seemingly contradictory, both of these features can be accounted for by using the simple line-of-centers model presented to explain earlier results for the Cl+CH$_4$ reaction. In contrast to the Cl+CH$_4$ reaction, the data suggest that the Cl+C$_2$H$_6$ reaction proceeds through a loosely constrained transition-state geometry. The reactions of atomic chlorine with ethane, C$_2$H$_6$, and perdeuteroethane, C$_2$D$_6$, yield virtually identical results. These findings, along with the low energy deposited by the reaction into the ethyl product (200±120 cm^{-1}), demonstrate that the alkyl fragment acts largely as a spectator in this hydrogen abstraction reaction. © *1996 American Institute of Physics.* [S0021-9606(96)00341-8]

I. INTRODUCTION

A microscopic understanding of bimolecular chemical reactions requires investigation of the conditions under which the two reagents come together, the forces that mediate reagent interaction, and the nature of the products formed. The rigor pursued in the description of a reaction varies greatly. A few reactive systems have been explained in great detail through the use of theoretical calculations on *ab initio* potential energy surfaces. In contrast, many single or related groups of reactions are understood through quasi-classical, classical, or even nonquantitative intuitive models. The present investigation aims to provide data necessary for both rigorous and intuitive descriptions. Our experimental approach is to measure the state-specific angular scattering distributions for a bimolecular reaction product. The resulting picture of product motions leads immediately to a physical understanding of the reactive process, and the quantitative data allows direct comparison with the results of theoretical studies.

This paper presents correlated state and scattering measurements for the gas-phase reaction of ground-state chlorine atoms with ethane molecules to produce hydrogen chloride and ethyl radicals

$$Cl(^2P_{3/2}) + C_2H_6 \rightarrow HCl + C_2H_5.$$
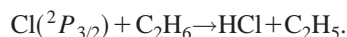
Kinetic studies have established this reaction to be slightly exothermic by 2.65 kcal/mol (928 cm^{-1}, 0.115 eV), with a rate constant of 5.9×10^{-11} cm^3 molecule^{-1} s^{-1} at 298 K.[1] No theoretical or experimental investigations have detailed the microscopic dynamics of this reactive system. Indeed, few reactions involving polyatomics have been studied from a dynamical standpoint. In an atom/diatom reaction (the traditional domain of reaction dynamics), a small number of experimental variables need to be constrained and a few

properties of the products need to be measured. Nonetheless, extreme diligence is required for detailed studies of such systems; complete product state and scattering information has been achieved in only a few cases, for example F+H$_2$ (Refs. 2 and 3) and H+H$_2$.[4,5] The large number of degrees of freedom in an atom/polyatom reaction magnifies the difficulty of the problem and usually results in a reduced degree of information obtained compared with these benchmark atom/diatom reactions.

After providing an experimental overview, we present HCl product state distributions and state-resolved angular distributions. Spatial anisotropy measurements are then discussed as a means of determining the average energy deposited into the unobserved C$_2$H$_5$ product. We briefly present data concerning how the scattering changes with product rotation and compare the Cl+C$_2$H$_6$ reaction with its fully deuterated analog. A simple, intuitive, and self-consistent model is presented to explain these results. Comparisons with other reactions of hydrocarbons with atomic chlorine are made, including an extended discussion of the closely related Cl+CH$_4$ reaction.

II. EXPERIMENT

The experimental apparatus and techniques have been described elsewhere, and a brief overview is detailed here. Molecular chlorine (Matheson Gases, 99.999%), ethane (Matheson Gases, 99.99%), and helium carrier gas (Liquid Carbonic, 99.995%) are premixed in a Teflon-lined tank. If shielded from light, this mixture does not produce significant amounts of HCl even when allowed to stand for days. The mixture is then fed through Teflon coils maintained at −78.5 °C (dry ice/ethanol mixture) to remove impurities produced by metal corrosion or reaction with pump oils or

greases; the gas mixture is then immediately coexpanded through a pulsed nozzle (General Valve 9-Series, 0.6 mm orifice) at 380 Torr backing pressure.

The reaction is initiated by photolysis of Cl$_2$ at 355 nm using the third harmonic of a Nd^{3+}:YAG laser. At this frequency, more than 98% of the chlorine atoms are produced in their ground state (Cl $^2P_{3/2}$);[6] consequently, almost all are moving at a single speed of 1680 m/s. The molecular chlorine precursor and the ethane molecules are assumed by virtue of translational cooling in a jet expansion to have very little motion with respect to each other. Therefore, the photolysis defines the relative motion between the chlorine atom and ethane molecule reagents, which produces a narrow distribution of center-of-mass collision energies for the reaction at 1900 cm^{-1} with a 420 cm^{-1} Gaussian spread (FWHM). This spread, which results from residual thermal motion of the jet-cooled reagents, is calculated using a 15 K translational temperature.[6] This value is a conservative estimate based on the measured 15 K rotational temperature of contaminant HCl in the expansion.

HCl products are allowed to build for 50–100 ns before they are detected with rovibrational state specificity via (2+1) REMPI through the F $^1\Delta_2$ state[7–11] or the f $^3\Delta_2$ state.[7–9] Frequency-doubled light at 240–243 nm from a Nd^{3+}:YAG-pumped dye-laser system (Spectra-Physics DCR 2A and PDL-3; Exciton, LD489 dye) drives the REMPI process at the focus of a 50 cm lens. The photolysis laser is more gently focused to a 1 mm beam diameter. Neither chlorine atoms nor reactive products are moving rapidly enough to traverse the photolysis beam radius on the time scales allowed for reaction; therefore, chlorine atom densities are constant in time, and reactive product concentrations build linearly after photoinitiation of the reaction. A slight correction accounting for the Gaussian profile of the photolysis beam is applied to speed-sensitive measurements of the product. A linear time-to-flight (TOF) mass spectrometer enables the separation of resonantly produced H^{35}Cl$^+$ and H^{37}Cl$^+$ from a variety of other background ions. Integration of the total H^{35}Cl$^+$ signal as the REMPI wavelength is scanned over the HCl excitation spectrum results in the product state distribution from the reaction, after correction by empirical linestrength factors.[11–14]

Measurement of the HCl speed distribution is accomplished using the method of core extraction, which has been described extensively by Simpson *et al.*;[15] a thumbnail sketch is provided here. HCl products are formed with some nascent distribution of velocities, determined by the initial speed of the reagents and the scattering behavior of the system, as described below. The photoionization process imparts virtually no velocity to the created ions, so that the initial speeds of the HCl$^+$ to be detected mirror those of the neutral precursors. The ion velocities create a spread in the ion packet as the packet travels in the mass spectrometer toward the detector. Faster velocities spread more, and slower ones less, as in a Doppler profile. The mass spectrometer is of Wiley–McLaren design[16] and is operated under space-focusing and velocity-sensitive conditions; therefore, this ion profile can be inverted directly to the original HCl speed distribution. This method can be used to obtained the entire three-dimensional velocity distribution through the use of the core extractor, a mask that is placed in front of the detector and rejects products scattered off the detection axis.

The lab-frame velocity of the reaction product is the vector sum of the center-of-mass velocity and the center-of-mass-frame product velocity. The former is determined by the coexpansion of reagents and the single-channel photolysis, as detailed earlier; the latter is determined by the energetics of the reaction, the selection of the product HCl internal energy state to be measured, and an assumption about the internal energy deposited into the unobserved C$_2$H$_5$ product. The determination of these two vectors, along with the measurement of the third, uniquely defines all angles of the triangle formed, in particular, the center-of-mass scattering angle. Thus, the measured lab-frame speed distribution is transformed into the center-of-mass distribution of scattering angles, which yields the state-resolved differential cross section for the reaction. This method for measurement of the differential cross section, which we call the *photoloc* method, has been used successfully by several investigators for an increasing number of reactive systems.[4,13,17–24]

Calculation of the differential cross section is predicated on the assumption of the internal energy of the unobserved product. Although this assumption is usually correct for atom/diatom systems, polyatomic reagents lead to polyatomic products, and one goal of the experiment is to understand the dynamical participation of both products. Making assumptions about the behavior of the unobserved product is therefore unsatisfying; furthermore, the increased number of degrees of freedom of a polyatomic product make these assumptions likely to be faulty. Therefore, a further measurement is performed to determine the angle between the center-of-mass velocity and the product lab-frame velocity. This angle allows a second use of the law of cosines to determine the center-of-mass product velocity without the need for assumptions. Unfortunately, this angle cannot be measured exactly in the current experiment. An averaged quantity related to this angle is obtained, however, in the measurement of the spatial anisotropy of the HCl product. This measurement is carried out by changing the linear polarization direction of the photolysis beam on alternate photolysis laser shots so that the electric vector of the photolysis light lies either parallel or perpendicular to the time-of-flight axis. The polarization flipping is effected by synchronization to the stress cycle of a photoelastic modulator (Hinds International, PEM-80), and the resulting polarizations have a transmittance ratio of at least 16:1 through a linear polarizer.

III. RESULTS

A. Rotational state distributions

HCl REMPI spectra were recorded on R- and S-branch transitions of the $F-X(0,0)$ band and Q-branch transitions of the $f-X(0,0)$ band, with total $m/z=36$ (H^{35}Cl$^+$) ion signal collected and integrated. The signals in these spectra were converted to populations using previously published correction factors[11–13] for the F $^1\Delta_2$ state and correction factors for
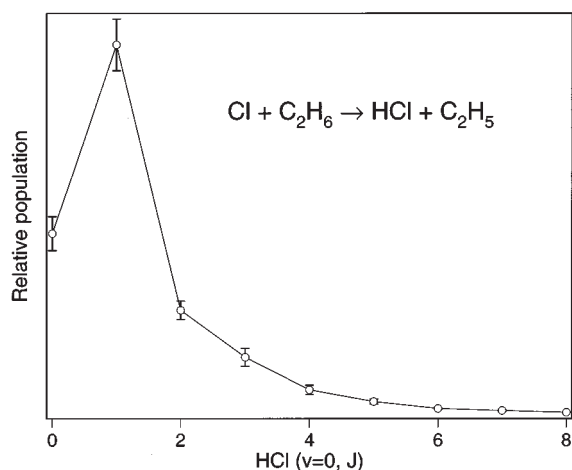
FIG. 1. Plot of the state distribution for the HCl ($v=0,J$) product from the reaction of atomic chlorine with ground-state ethane. Error bars represent 1σ statistical deviations. Relative populations are determined from REMPI spectra as described in the text.

FIG. 2. The energetics of the reaction of atomic chlorine with ethane. The collisional energy spread is calculated following van der Zande *et al.*[6] assuming a 15 K beam translational temperature.

the $f\ ^3\Delta_2$ state obtained from thermal HCl spectra.[14] The HCl($v=0,J$) product rotational state distribution from the Cl+C$_2$H$_6$ reaction is presented in Fig. 1, which shows a cold rotational distribution with 48 ± 3 cm^{-1} average energy in rotation. Levels of contaminant HCl present in our gas mixture before reaction were small compared with signal magnitudes; this contamination was eliminated from the collected signal through the use of photolysis on/off subtraction. The photolysis laser was operated at half the repetition rate of the probe, which allowed subtraction of signals on an every-other-shot basis. Because most backgrounds, including contaminant HCl, did not rely on the presence of the photolysis laser, they were thus eliminated by this subtraction procedure. Because the reactive signal depends on the photolysis for the production of the chlorine atom reagent, the result of the on/off subtraction is to separate the reactive signal from possible background interference. The photolysis laser alone caused no ionization.

The time dependence of product formation was measured to check the nascency of the state distribution. We verified that for several rotational states across the distribution, the state distribution did not vary with the time delay between reaction initiation and product probe on the timescales allowed for reactive product buildup. Additionally, products were seen to build linearly with this delay, as is expected at short delays during which reagent chlorine concentration does not change. The intercept of this linear growth could be extrapolated to zero product at laser overlap. Thus, we have seen no evidence of either HCl product relaxation or HCl formation from photodissociation of possible Cl$_2$/C$_2$H$_6$ clusters.

Vibrationally excited HCl($v=1$) was also observed as a reaction product. This product state is not strictly energetically allowed, as shown in Fig. 2, but it is permissible within our spread of collision energies. We measured the ratio of HCl($v=0$):HCl($v=1$) populations to be 300:1. Given the amount of population and the nearness of this channel to
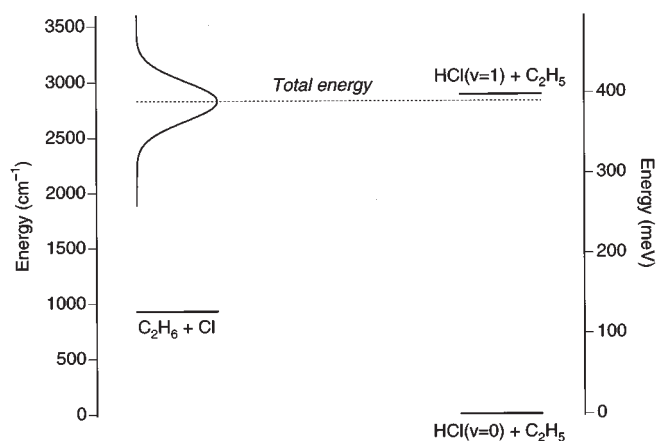
threshold, other sources of formation cannot be discounted, especially reaction of ethane with Cl($^2P_{1/2}$) present as 2% of our atomic chlorine reagent. Therefore, results for HCl($v=1$) cannot be made quantitative at this time.

B. Speed distributions and angular scattering

In the measurement of ion-arrival-time profiles for the determination of speed distributions and thus differential cross sections, removal of background was accomplished using time-jump subtraction. In this subtraction procedure, the photolysis/probe time delay is alternated every 20 laser shots between two values: A short time delay for which background contributions and very little reactive signal are present, and a longer time delay with the same background contributions and more signal allowed to build up. This differencing procedure results only in signals that change with delay between photolysis and probe laser pulses, which eliminates essentially all background interference from the measurement of reactive signal. This more rigorous subtraction procedure is necessary for velocity-sensitive detection, in which quickly moving H^{35}Cl$^+$ overlaps at the detector with both ^{35}Cl$^+$ and ^{37}Cl$^+$ backgrounds. Additionally, for small signals [HCl($v=0$, $J=6$) and HCl($v=0$, $J=8$) products] photolysis and probe-induced C$_2$H$_n^+$ background contributions necessitated a linear baseline correction for arrival profiles.

The three-dimensional velocity distribution of the HCl product is determined using core-extracted ion-arrival-time profiles. Two distinct profiles were recorded for each product state: One with the photolysis laser polarization perpendicular to the flight axis, referred to as I_{perp}; the other with the polarization parallel, referred to as I_{par}. These profiles were recorded concurrently, with the polarization alternating every other laser shot. The Cl$_2$ photolysis, which has a pure sin$^2\theta$ distribution ($\beta=-1$) for Cl($^2P_{3/2}$) at this frequency,[25] is the only source of anisotropy in the experiment. Therefore, measurements at any two polarizations contain all of the information describing the three-dimensional velocity distribution
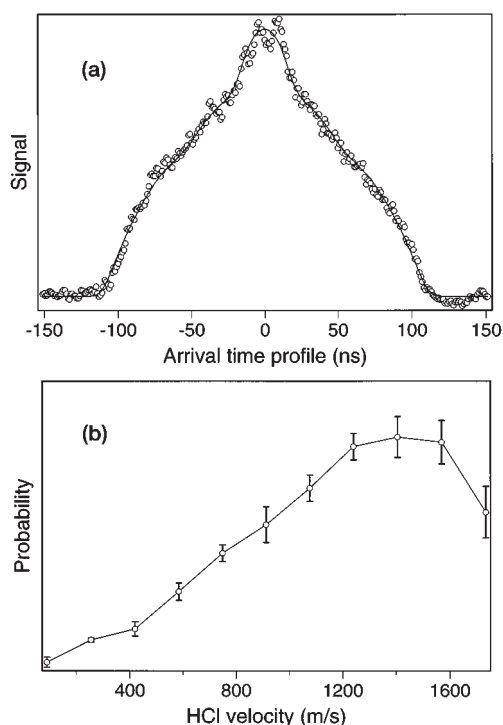
FIG. 3. (a) Core-extracted ion-arrival profile for HCl (v=0, J=1), along with the calculated best fit function. Spatial anisotropy has been removed by forming a composite profile from the isotropic sum, $I_{iso}=I_{par}+2I_{perp}$ of profiles measured with the photolysis polarization parallel and perpendicular to the TOF axis. (b) Speed distribution of HCl (v=0, J=1) resulting from a maximum-entropy analysis that fits the arrival profile to a combination of instrumental basis functions. Error bars represent 1σ statistical deviations of replicate measurements.

FIG. 4. Differential cross section for the reactive product HCl (v=0, J=1), calculated from the measured speed distribution shown in Fig. 3. The calculation requires an assumption of the C$_2$H$_5$ internal energy. For this analysis, the ethyl fragment is assumed to take negligible energy into internal modes; this assumption is discussed extensively in the text.

of the product. Analysis of these time profiles is accomplished in two steps through the formation of two composite profiles. The first composite profile I_{iso} is formed as the sum $I_{par}+2I_{perp}$. This sum removes all spatial anisotropy from the data and is thus analyzed straightforwardly to yield the speed distribution. The second composite profile I_{aniso} contains the anisotropic component of the spatial distribution and is analyzed in Sec. III C to yield the speed dependence of the second Legendre moment, β_{prod}.

Figure 3(a) shows the core-extracted composite time profile I_{iso} for HCl(v=0, J=1) product from the Cl+C$_2$H$_6$ reaction, recorded with a 62 V/cm extraction field. The data were analyzed in a fashion similar to that described previously.[15] A set of basis functions, each describing the instrumental response to a monoenergetic speed distribution, was constructed and calibrated to Cl atoms at known speeds. Owing to the slow product speeds possible for this reaction, further calibration was performed using Cl($^2P_{1/2}$) from 481 to 491 nm photolysis of Cl$_2$(v=1);[25] this photolysis produced monoenergetic speed distributions tunable between 130 and 400 m/s. Basis functions were constructed for photolysis polarizations parallel and perpendicular to the TOF axis. Composite isotropic and anisotropic basis functions, analogous to the isotropic and anisotropic profiles, were then used to fit the data. Profiles were fit to a linear combination of basis functions using a maximum-entropy analysis;[15,18]
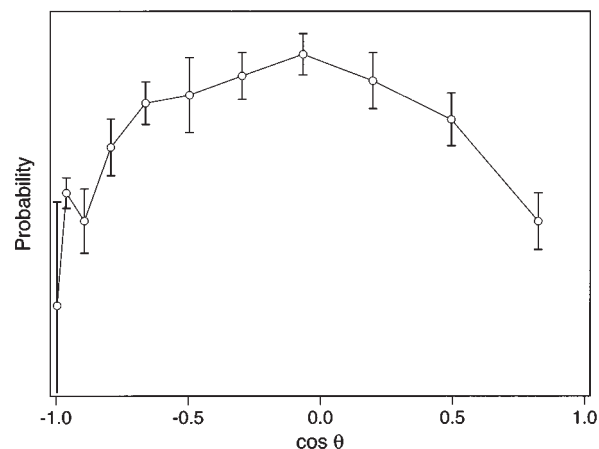
these basis functions were chosen to be equally spaced in speed, which reflects the experimental resolution. The resulting speed distribution for HCl(v=0, J=1) product is shown in Fig. 3(b); the 1σ error bar for each speed is determined from statistical variation in replicate measurements.

The reaction is able energetically to populate speeds ranging from 0 to 1815 m/s. The speed distribution shows a small amount of slowly moving product, increasing steadily to a maximum near the fastest speeds allowable. For the moment we make the assumption, supported later, that the C$_2$H$_5$ fragment takes none of the energy available to the reaction into internal excitation. Using this assumption, we can easily convert the product speed to the center-of-mass scattering angle, as explained earlier. Figure 4 shows a plot of the differential cross section against the cosine of the scattering angle. The uneven spacing of the points in this graph along the cos θ axis makes the nonlinearity of this conversion evident and emphasizes that while the experimental resolution is constant in speed, it varies with respect to cos θ. The associated volume element for this conversion is what transforms a large preference for the formation of faster over slower products into nearly equal amounts of forward-scattered (cos θ=1) and backward-scattered (cos θ=$-$1) products.

Note that large product rotational alignment effects, if present, would complicate this analysis and must be evaluated along with the speed distribution.[26–28] Small HCl velocity/rotation vector correlations have been observed in the Cl+CH$_4$ system.[29] These correlations are determined experimentally through changes in core-extracted time profiles dependent on the REMPI probe laser polarization. We have performed probe polarization-flipping experiments on several HCl product states for Cl+C$_2$H$_6$ and have observed measurable but very small changes in the time profiles ($\approx$5%). These changes are small enough to be ignored for purposes of determining speed and anisotropy distributions.
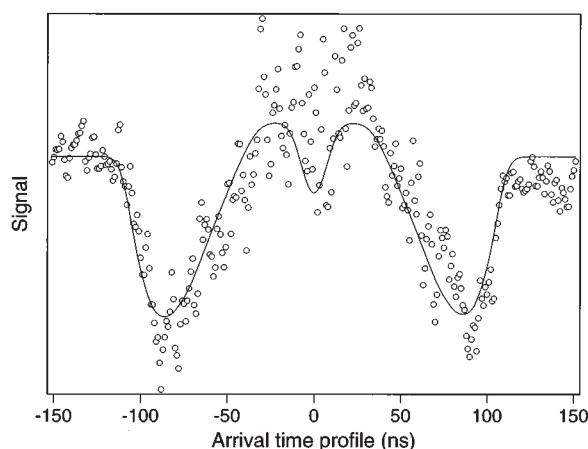
FIG. 5. Core-extracted ion-arrival profile for HCl ($v=0$, $J=1$). This profile is a composite that contains product spatial anisotropy information; the profile is generated as twice the anisotropic difference of experimental profiles measured with the photolysis polarization parallel and perpendicular to the TOF axis, $I_{aniso}=2(I_{par}-I_{perp})$. The solid line shows the fit to the data as a sum of instrumental basis functions obtained through a least-squares fitting algorithm.
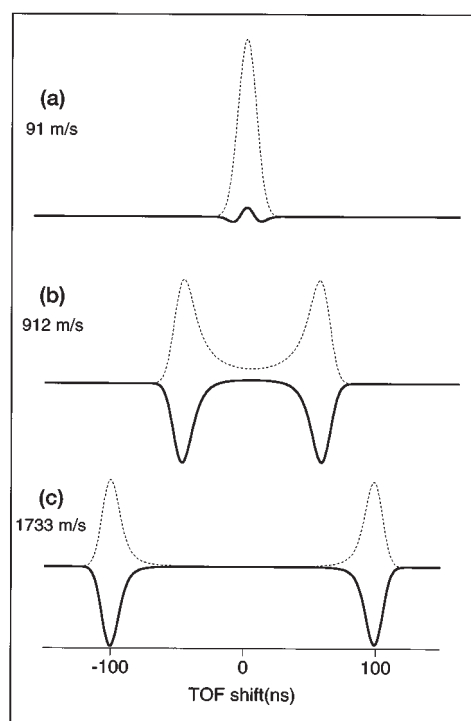

FIG. 6. Three representative basis functions that predict instrumental response for a composite anisotropic profile for single-speed products at 91, 912, and 1733 m/s, all with spatial anisotropy $\beta=-1$. The basis functions showing instrumental response to isotropic profiles for each speed are shown as dotted lines to demonstrate sensitivity to anisotropy.

C. Speed-dependent spatial anisotropy

The composite core-extracted time profile $I_{aniso}=2(I_{par}-I_{perp})$ for HCl($v=0$, $J=1$) is shown in Fig. 5. This profile is once again fit to a linear combination of basis functions. These basis functions are anisotropic composites of parallel and perpendicular bases and mimic the instrumental sensitivity to product spatial anisotropy. Three representative functions are shown in Fig. 6, along with corresponding isotropic basis functions. The sensitivity to spatial anisotropy is strongest at high speeds, as evidenced by the large, sharply peaked form of the fastest anisotropic basis function. The core extractor causes this behavior at these product speeds by preferentially selecting products with little velocity transverse to the detection axis. The slower product speeds are less effectively discriminated, and the sensitivity to anisotropy is correspondingly decreased. Fitting to the profile I_{aniso} was accomplished using a Levenburg–Marquart nonlinear least squares algorithm,[30] which determined the first two or three Legendre moments of the speed-dependent spatial anisotropy. Alternate analyses yield nearly identical results. Figure 7 shows the result of the least squares Legendre fit, along with replicate measurement 1σ error bars. This plot of spatial anisotropy describes the product spatial distribution as a function of lab-frame speed,

$$I(v_{HCl}, \theta_{phot}) = \frac{d\sigma}{dv_{HCl}}[1+\beta(v_{HCl})P_2(\cos\theta_{phot})], \quad (1)$$

in terms of the angle θ_{phot}, which is defined relative to the polarization vector of the photolysis laser. The quantity $\beta(v_{HCl})$ is plotted against v_{HCl} in the figure.

Consider HCl products in a measured internal state (v,J) with a measured lab-frame speed v_{HCl}; the center-of-mass speed v_{com} is determined by the reagent speed and

relative reagent masses. If the center-of-mass scattering angle θ_{com} were known, the product speed in the center of mass frame u_{HCl} could be calculated from

$$u_{HCl} = [v_{HCl}^2 - v_{com}^2(1-\cos^2\theta_{com})]^{1/2}$$
$$- v_{com}\cos\theta_{com}, \quad (2)$$

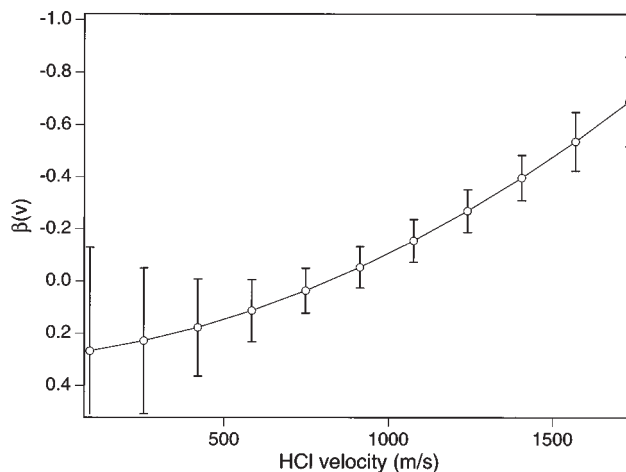so that θ_{lab} is given by

FIG. 7. HCl ($v=0$, $J=1$) product spatial anisotropy as a function of speed, $\beta(v)$, resulting from analysis of the anisotropic time profile shown in Fig. 5. Error bars represent 1σ statistical deviations of replicate measurements.
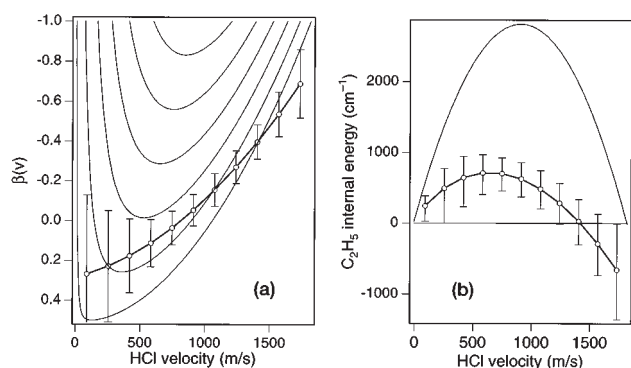
FIG. 8. (a) HCl product spatial anisotropy as a function of speed, as in Fig. 7, with added contours that indicate the calculated relationship between β and v for varying degrees of C$_2$H$_5$ internal excitation. The outermost curve shows the predicted form for $\beta(v)$ assuming no C$_2$H$_5$ internal excitation; inner contours are spaced by 500 cm^{-1} in ethyl excitation. (b) C$_2$H$_5$ internal energy excitation plotted as a function of HCl velocity. This plot results from a transformation of the data shown in Fig. 8(a), as detailed in the text.

$$\cos\ \theta_{lab} = \frac{v_{HCl}^2 + v_{com}^2 - u_{HCl}^2}{2v_{HCl}v_{com}}, \tag{3}$$

where θ_{lab} is the angle between the lab-frame velocity, v_{HCl}, of the HCl product and the center-of-mass velocity, v_{com}, which lies along the velocity of the Cl reagent. Thus, HCl product at a given speed u_{HCl} and center-of-mass scattering angle θ_{com} appears in the laboratory with angle θ_{lab} in a cone about every Cl reagent velocity. This analysis leads to an expression for the spatial anisotropy of the product

$$\beta_{HCl}(v_{HCl}) = \beta_{Cl}P_2(\cos\ \theta_{lab}). \tag{4}$$

Thus, we see that knowledge of the center-of-mass scattering angle allows direct calculation of the lab-frame anisotropy and the center-of-mass velocity. Because in most cases multiple scattering angles are possible for a given value of the measured speed v_{HCl}, β_{HCl} is an inherently averaged quantity that cannot be inverted to yield the scattering angle or center-of-mass velocity without further knowledge of the distribution of angles averaged. The measurement of $\beta(v)$ through the use of anisotropic core-extracted time profiles nonetheless provides dynamical insight into the behavior of the C$_2$H$_5$ product.

An assumption of the energy present in C$_2$H$_5$ internal modes, along with the measurement of the HCl internal state and the known energetics of the system, determines the energy available for kinetic release into products and thus the magnitude of the center-of-mass speed u_{HCl}. This assumption fixes the relation between β and v, and in Fig. 8(a), $\beta(v)$ contours for varying degrees of ethyl excitation have been placed over the experimental data. The anisotropy data overlaps the outermost contours, indicating that very little energy from the reaction appears in the internal modes of the C$_2$H$_5$ radical. Alternately, by inverting Eq. (4) and applying Eqs. (2) and (3), we can convert the measured anisotropy into an average C$_2$H$_5$ internal energy. Essentially, this procedure results in a change in coordinates that transforms Figs. 8(a) to 8(b), a plot of ethyl energy as a function of HCl
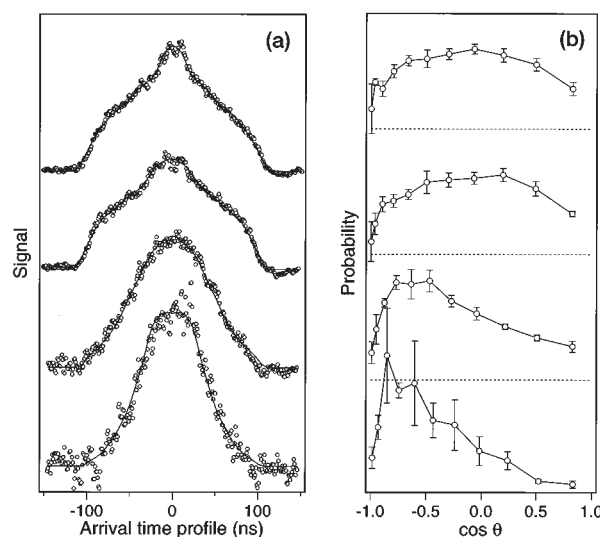

FIG. 9. Ion arrival profiles and differential cross sections for HCl ($v=0$) products: $J=1$, $J=3$, $J=6$, and $J=8$. The profiles are narrower at higher rotational levels, which indicates slower product velocities and thus a trend toward back-scattering in the differential cross section.

product speed. In Fig. 8(b), the inverted parabola is drawn to show the amount of available energy not appearing in product translation. Averaging the internal energy for each speed, weighted by the measured speed distribution, yields a C$_2$H$_5$ internal energy of 200 ± 120 cm^{-1}. This low degree of internal excitation justifies the assumption made earlier in transforming the speed distribution into the differential cross section. Similar measurements of product internal excitation through spatial anisotropy measurements have been performed for several other systems.[5,13,21] The treatment presented here allows for direct inversion of the data to produce $\beta(v)$, as contrasted with methods that assume internal excitation and then forward convolute to fit anisotropy data.

D. Speed distribution dependence on product rotation

The analysis detailed in Secs. III B and III C has concerned a single product state, HCl ($v=0$, $J=1$), populated by the Cl+C$_2$H$_6$ reaction. These data were presented first and most comprehensively because HCl product is most likely to be formed in this state (see Fig. 1). One of the strengths of the photoloc technique, however, is its ability to measure speed distributions with complete product state selectivity. Figure 9 presents the isotropic core-extracted time profiles for HCl($v=0$,J) for $J=1$, $J=3$, $J=6$, and $J=8$; the corresponding state-resolved differential cross sections resulting from analysis, again assuming no C$_2$H$_5$ excitation, are shown alongside each profile. The speed distributions from which these cross sections were derived were verified as nascent by ascertaining that the profiles did not change between very short photolysis/probe time delays and the delays used to acquire the data shown. The $J=1$ and $J=3$ profiles are similar, and this similarity is reflected in nearly identical differential cross sections for these states. A marked change in the
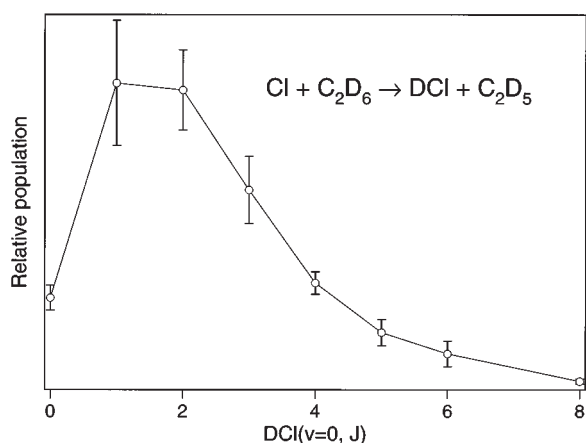
FIG. 10. Rotational state distribution for the DCl ($v=0,J$) product from the reaction Cl+C$_2$D$_6$→DCl+C$_2$D$_5$. Error bars represent 1σ statistical deviations of replicate measurements. A slight propensity for higher rotational states is seen, as compared with the nondeuterated reaction.

shape of the core-extracted profiles occurs, however, for the higher rotational states, which upon analysis corresponds to a shift toward increased back-scattering.

E. Reaction with C$_2$D$_6$

Similar measurements to those described in the preceding sections on the Cl+C$_2$H$_6$ reaction were performed for the fully deuterated isotopomer. Significant changes in zero-point energy make this reaction nearly thermoneutral, $\Delta E = -0.3$ kcal/mol.[31] The DCl ($v=0$) rotational state distribution is shown in Fig. 10. Owing to the decreased exothermicity of the deuterated reaction, DCl($v=1$) formation is once again at the energetic threshold, and although it is observed, the same problems are present as with HCl($v=1$) product from Cl+C$_2$H$_6$. The state distribution was recorded on the R and S branches of the $F(0,0)$ band of DCl and converted to populations using correction factors determined experimentally from spectra of thermal DCl samples. DCl is formed in higher rotational states than HCl for the analogous reaction. However, the average rotational energy of the DCl product, 51 ± 4 cm^{-1}, is similar to the value for HCl, 48 ± 3 cm^{-1}. The analogous result of higher rotational states but equal rotational energies was observed for the Cl+CH$_4$ and Cl+CD$_4$ systems.[24] The scattering of the DCl product from Cl+C$_2$D$_6$ is very similar to that of HCl from Cl+C$_2$H$_6$. Once again, the spatial anisotropy indicates that very little excitation appears in the C$_2$D$_5$ fragment. The trend of increased back-scattering with higher rotational states is also observed for the reaction with perdeuterated ethane.

IV. DISCUSSION

The reaction of atomic chlorine with ethane has been studied using a photoinitiated scheme that allows the measurement of nascent state distributions and state-resolved differential cross sections for the HCl product, as well as the average internal energy of the C$_2$H$_5$ product associated with each measured product state. The HCl($v=0$) product is formed with little rotational excitation and scatters nearly isotropically in the center-of-mass frame, with a trend toward increased back-scattering with increasing HCl rotation.

A possible interpretation of the HCl ($v=0$, $J=1$) differential cross section would attribute the broad scattering, with a slight peak at side-scattering and somewhat symmetric drop in the forward and backward direction, to a complex-forming mechanism that dissociates to products parallel to the rotational axis of the complex.[32] This interpretation is unsatisfying. The Cl+CH$_4$ and Cl+C$_2$H$_6$ systems are similar in many ways, and the differences do not seem so severe as to warrant an abrupt and complete changeover from direct to complex dynamics. More importantly, complex mechanisms usually involve considerable randomization of energy into internal modes of the products. The extremely cold HCl rotational distribution, which takes only 2% of the available energy into rotation; and the low degree of C$_2$H$_5$ internal excitation, which takes 7%, indicate direct dynamics for this reaction.

Additional insight into the dynamics of the Cl+C$_2$H$_6$ system can be obtained from the speed-dependent anisotropy, analysis of which yields the average C$_2$H$_5$ internal excitation. The result, that the reaction deposits little internal energy into the ethyl radical product, not only allows for inversion of speed to scattering but furthermore suggests that the ethyl radical has little effect on the dynamics of the reaction. This conclusion is further supported by close similarities between the reactions of chlorine atoms with C$_2$H$_6$ and C$_2$D$_6$ as the dynamical effect by the ethyl radical would be expected to change with complete deuteration. Characterization of the reaction as an atom/pseudo-diatom system, Cl+RH(D), in which the alkyl acts as a spectator, seems to be borne out by these data. The ability to make this simplification is of key interest for attempts to model this and larger reaction systems.

One model of chemical reactivity holds that product rotational excitation results from an impulsive release of energy into products from a bent transition state. Under this model, a linear transition state, where transition state angles are restricted to small deviations, results in little product rotation; furthermore, linear transition states are assumed to produce a preference for product back-scattering. This three-way correspondence between a cold rotational distribution, a linear transition state, and backward scattering was developed for and has been applied to a wide number of atom/diatom systems. For atom/polyatom systems, such as Cl+C$_2$H$_6$, transition-state forces can be more complex, and application of an impulsive release model requires further assumptions. A simple treatment is to model the polyatomic molecule as a pseudo-diatomic, for example Cl+H–C$_2$H$_5$. Thus, by assuming that energy is released along the C–H bond, the linearity of the Cl–H–C bond can be related to the final product rotational distribution.

State distributions for several Cl+hydrocarbon reactions have been published. Distributions from methane, propane, and isobutane were reported by Varley and Dagdigian;[33] propane was reported by Koplitz and co-workers;[34] and perdeuterated cyclohexane by Flynn and co-workers.[35] In all cases,

rotational excitation of the product was extremely low. Based on an impulsive release model and analogy to Cl+CH₄, for which a linear transition state is calculated,[35,36] these rotational state distributions were used to predict transition states for Cl+hydrocarbon reactions and to explain measured product back-scattering for Cl+C₄H₁₀.[33] This prediction is verified for Cl+CD₄, for which members of our laboratory measured a cold rotational distribution and complete back-scattering for the DCl product.[24] In light of these data, the cold rotational distribution and broad, nearly isotropic scattering evidenced by Cl+C₂H₆ seem surprising, though they are similar to recent state and scattering measurements on Cl+isobutane.[37] We present an alternate model for Cl+C₂H₆ reactivity that explains how isotropic scattering is consistent with low HCl rotational excitation; furthermore, the model presented is a direct extension of the model used to explain Cl+CD₄ dynamics.

A. Line-of-centers model

Further insight into how a reaction scatters isotropically with little rotational excitation is gained through analogy to the correlated state and scattering measurements of the vibrationally excited reaction Cl+CH₄ (v_3=1).[13] The HCl (v=1) product from this reaction is no more rotationally excited than HCl(v=0) from Cl+CH₄ (v=0). In contrast to the backward-scattering seen for the products from ground-state methane, the vibrationally excited products scatter with a distribution peaked sharply in the forward direction. These products were posited to result from a nonimpulsive stripping mechanism that originated from collisions at large impact parameters that provided little or no torque to the departing molecule. This system was proposed to show such a radical difference in behavior as a consequence of the vibrational excitation of the reagent. The physical model presented suggested that the vibrational excitation removed or significantly lowered the barrier to reaction; a later quasiclassical trajectory study of this reactive system required a slight well in the potential surface to reproduce the experimental results.[38] In a similar fashion, a small reactive barrier for the Cl+C₂H₆ reaction could allow analogous nonimpulsive stripping for a vibrationally unexcited reaction, resulting in forward-scattered product and low rotational excitation. The barrier to the reaction is not known, but analysis of kinetic data yields an activation energy of 70 cm⁻¹ at 220–600 K, which is 4% of the 1900 cm⁻¹ collision energy available to the system. We propose that this large excess of collision energy is what accounts for the striking differences in scattering between the Cl+C₂H₆ and Cl+CD₄ systems; the barrier height for the latter reaction is estimated at 1370 cm⁻¹, which is 90% of the 1495 cm⁻¹ collision energy.

The behavior of the Cl+CD₄ system was explained through the use of the line-of-centers model.[32] This model states that for an activated reaction, any given collision proceeds toward products if and only if the reactive barrier is exceeded by the collision energy along the line of centers of the reagents; motion transverse to this line does not affect the

reaction. This simple model results in a relation between reaction probability and impact parameter

$$E_T\left(1-\frac{b^2}{d^2}\right)\geq E_0, \tag{5}$$

where E_T is the reagent translational energy, E_0 is the barrier energy, and b is the impact parameter, normalized by a distance d at which reaction occurs. This equation can then be more broadly applied to yield a differential cross section, based on the hard-sphere relation between impact parameter and scattering angle, to produce the following equations;[24]

$$\frac{d\sigma}{d\cos\theta}=\begin{cases}\frac{1}{2}\,p\,\pi d^2, & -1\leq\cos\theta<\cos\theta_{max} \\ 0, & \cos\theta_{max}<\cos\theta\leq1\end{cases} \tag{6}$$

and

$$\cos\theta_{max}=1-\frac{2E_0}{E_T}. \tag{7}$$

These equations qualitatively describe the back-scattering observed for the Cl+CD₄ system, where $\cos\theta_{max}$=−0.83. The larger collision energy and smaller barrier for Cl+C₂H₆ in this experiment yield $\cos\theta_{max}$=0.93, essentially in agreement with the nearly isotropic scattering seen for the system. A modified version of the line-of-centers model that includes a barrier dependence on C–H–Cl transition state angle, as presented by Smith,[39] would predict a decrease in scattering intensity in the forward direction, in contrast to the step-function differential cross section described in Eq. (6). This prediction would model the experimentally observed scattering more accurately; however, quantitative comparison to this model requires knowledge concerning the C–H–Cl transition-state bending potential. Note that the simple line-of-centers model makes testable predictions concerning Cl+C₂H₆ scattering as a function of collision energy. The scattering is predicted to remain unchanged at higher collision energies, whereas lower collision energies are predicted to produce more side- and back-scattered distributions that, when the energy is comparable to the Cl+C₂H₆ barrier, will eventually mirror the complete back-scattering seen in the Cl+CD₄ reaction. Because of the low activation barrier and the relatively high collision energy for the Cl+C₂H₆ reaction, the role of the ethane molecule is essentially that of a ''ball of hydrogens''; regardless of where the chlorine impacts the ethane, a hydrogen atom can be successfully abstracted.

B. HCl rotation and the Cl-H-C₂H₅ transition state

The transition state for the Cl+CH₄ reaction has been predicted to be linear based on *ab initio* calculations,[35,36] and a narrowly constrained geometry is indicated by the small preexponential factor in the thermal rate expression.[1] A similar calculation shows the Cl+C₂H₆ transition state to be linear.[40] A first assessment might predict this geometry to be tightly constrained based on the chemical similarities between CH₄ and C₂H₆. However, the preexponential factor is eight times greater for the Cl+C₂H₆ reaction,[1] which pre-

dicts looser steric requirements at the transition state. Under the nonthermal conditions of this experiment, the $Cl+C_2H_6$ reaction produces hundreds of times more HCl product than was seen in previous studies of the $Cl+CH_4$ reaction. Although this ratio cannot be made quantitative because of differences in the nozzle expansion, we conclude that ethane is far more reactive than methane, beyond the extent explainable by the differences in product scattering between the two systems. For any scattering angle, and for any HCl product state, the interaction of chlorine atoms with C_2H_6 is more likely to proceed toward reaction than for CH_4. We draw the conclusion, based on thermal rate data and the observed magnitude of our signals, that a larger proportion of the $Cl+C_2H_6$ potential energy surface is reactive—that is, the reaction proceeds through a ''loose'' transition state.

While a loose transition state and broad, near-isotropic scattering are in accordance with a large thermal rate for the $Cl+C_2H_6$ reaction, these must be reconciled with the extremely cold measured product rotational distribution. Simple models of reactivity describe the rotational excitation of the product as the result of an impulsive ''push'' at the transition state. These models suggest that a cold rotational distribution indicates that the C–H–Cl bond is always linear at the transition state, resulting in little or no torque concomitant with product formation. This strict geometrical constraint is at odds with the observed reaction rate. A similar discrepancy was discussed for the $Cl+C_6D_{12}$ (deuterated cyclohexane) reaction by Flynn and co-workers,[41] who also measured cold DCl product rotational temperatures. For that system, it was suggested that low-frequency modes of the hydrocarbon reactant could allow a large thermal rate and a linear transition state. Under this model, the zero-point motion associated with C–D bending modes was posited to be sufficient to bring the reactants into a linear configuration for a large percentage of collisions. This model could be applied to $Cl+C_2H_6$ but does not explain in a fully satisfactory fashion why similar C–H motions in the $Cl+CH_4$ reaction result in a far smaller thermal rate.

We submit an alternate explanation wherein products are formed without impulsive release. The connection between transition-state bend angle and product rotation results from a model involving sudden forces at the transition state. This connection is complicated by forces of longer duration or of longer range than are normally considered in the domain of the reaction transition state. Therefore, any reactive mechanism that does not require a sudden force on the departing hydrogen atom allows low rotational excitation to result from a wide range of geometries.

Forward- and side-scattered products from $Cl+C_2H_6$ are assumed to result from near-miss and glancing impacts of the atomic chlorine on the ethane. Because very little of the translational energy is coupled into the reaction coordinate for these trajectories and because these trajectories require only small deviations in the direction the chlorine atom travels as it abstracts hydrogen, the interaction necessary with the ethane potential is weak. This weak interaction allows hydrogen transfer to occur nonimpulsively in a manner similar to the stripping mechanism seen for $Cl+CH_4$ ($\nu_3=1$);[13]

consequently, the rotational distribution is cold. Note that this model attributes the cold rotational distribution of these products solely to the kinematics of the reactive collision and requires no assumptions of the transition-state geometry.

Trajectories that result in back-scattered products require stronger interactions, as the chlorine atom must abstract hydrogen from the ethane and then recoil from the ethyl radical. These products might be expected to be formed more impulsively. Back-scattered products are indeed correlated with higher rotational states, as can be seen from the rotational dependence of the differential cross section presented in Sec. III D. Even the back-scattered products, however, are not rotationally excited significantly compared with the total energy available to products. By assuming these products are formed impulsively, we can predict a strongly linear transition state geometry; however, a nonimpulsive mechanism and a geometrically unconstrained transition state are more in accordance with the observed reaction rate.

The chemical similarity of the $Cl+CH_4(CD_4)$ and $Cl+C_2H_6$ reactions is reflected in that both abstractions proceed via direct dynamics, and both are explained qualitatively by a simple line-of-centers model, indicating that reagent translational energy along the reactive Cl–H–C axis is effective in surmounting an energetic barrier to abstraction. Differences in product scattering are explained under this model as the direct result of a lower energetic barrier for the $Cl+C_2H_6$ reaction. We propose that the similarity in product rotational state distributions does not indicate similar geometric constraints for the two reactions, and we rely instead on thermal reaction rate measurements to predict a loose, geometrically unconstrained transition state for $Cl+C_2H_6$. This loose transition state is reconciled with the observed cold rotational distribution by the proposal of a reaction mechanism that does not involve significant impulsive release of energy into products. A further experimental verification of the differences between the $Cl+CH_4$ and $Cl+C_2H_6$ transition states is available in the study of the effect of reagent vibrational excitation on reactivity. Previous studies of $Cl+CH_4$ ($\nu_3=1$) have shown that the effect of vibrational excitation is to both lower the energetic barrier and to loosen geometrical constraints to reaction.[13,24] A similar study of the reaction of chlorine with vibrationally excited ethane is the topic of a forthcoming publication.

The preceding arguments show that no straightforward relationship necessarily holds between the reaction transition-state geometry and the measured rotational state distribution. The results presented in this paper also demonstrate that no simple correspondence exists between state and scattering distributions. We emphasize that both product state distributions and scattering information are necessary to determine the broader dynamics of the studied system.

ACKNOWLEDGMENT

[1] R. Atkinson, D. L. Baulch, R. A. Cox, R. F. Hampson, Jr., J. A. Kerr, and J. Troe, J. Phys. Chem. Ref. Data **21**, 1125 (1992).

[2] M. Faubel, B. Martinez-Haya, L. Y. Rusin, U. Tappe, and J. P. Toennies, Chem. Phys. Lett. **232**, 197 (1995).

[3] D. M. Neumark, A. M. Wodtke, G. N. Robinson, C. C. Hayden, and Y. T. Lee, J. Chem. Phys. **82**, 3045 (1985).

[4] H. Xu, N. E. Shafer-Ray, F. Merkt, D. J. Hughes, M. Springer, R. P. Tuckett, and R. N. Zare, J. Chem. Phys. **103**, 5157 (1995).

[5] L. Schnieder, K. Seekamp-Rahn, J. Borkowski, E. Wrede, K. H. Welge, F. J. Aoiz, L. Banares, M. J. D'Mello, V. J. Herrero, V. S. Rabanos, and R. Wyatt, Science **269**, 207 (1995).

[6] W. J. van der Zande, R. Zhang, R. N. Zare, K. G. McKendrick, and J. J. Valentini, J. Phys. Chem. **96**, 8205 (1991).

[7] D. S. Green, G. A. Bickel, and S. C. Wallace, J. Mol. Spectros. **150**, 388 (1991).

[8] D. S. Green, G. A. Bickel, and S. C. Wallace, J. Mol. Spectros. **150**, 354 (1991).

[9] D. S. Green, G. A. Bickel, and S. C. Wallace, J. Mol. Spectros. **150**, 303 (1991).

[10] S. Arepalli, N. Presser, D. Robie, and R. J. Gordon, Chem. Phys. Lett. **118**, 88 (1985).

[11] Y. Xie, P. T. A. Reilly, S. Chilukuri, and R. Gordon, J. Chem. Phys. **95**, 854 (1991).

[12] Y. Huang, Y.-A. Yang, G.-X. He, and R. J. Gordon, J. Chem. Phys. **99**, 2752 (1993).

[13] W. R. Simpson, T. P. Rakitzis, S. A. Kandel, A. J. Orr-Ewing, and R. N. Zare, J. Chem. Phys. **103**, 7313 (1995).

[14] Empirical linestrengths for the $f-X(0,0)$ Q branch were derived from spectra of thermal HCl, and show a decreased sensitivity at higher rotational levels with respect to two-photon linestrengths. Measured ion signal is multiplied by these correction factors to yield population [normalized to $Q(2)$]: $Q(2)$, 1.00; $Q(3)$, 1.11; $Q(4)$, 1.34; $Q(5)$, 1.81; $Q(6)$, 2.62; $Q(7)$, 3.72.

[15] W. R. Simpson, A. J. Orr-Ewing, S. A. Kandel, T. P. Rakitzis, and R. N. Zare, J. Chem. Phys. **103**, 7299 (1995).

[16] W. W. Wiley and I. H. McLaren, Rev. Sci. Instrum. **26**, 1150 (1955).

[17] G. E. Hall, in *Proceedings of Twelfth Combustion Research Conference* (The Combustion Research Facility of Sandia National Laboratory, Livermore, CA 1990)

[18] H. L. Kim, M. A. Wickramaaratchi, X. Zheng, and G. E. Hall, J. Chem. Phys. **101**, 2033 (1994).

[19] M. Brouard, S. P. Duxon, P. A. Enriquez, and J. P. Simons, J. Chem. Phys. **97**, 7414 (1992).

[20] F. J. Aoiz, M. Brouard, P. A. Enriquez, and R. J. Sayos, J. Chem. Soc., Faraday Trans. **89**, 1427 (1993).

[21] M. Brouard, S. P. Duxon, and J. P. Simons, Isr. J. Chem. **34**, 67 (1994).

[22] M. Brouard, S. P. Duxon, P. A. Enriquez, R. Sayos, and J. P. Simons, J. Phys. Chem. **95**, 8169 (1991).

[23] M. Brouard, S. P. Duxon, P. A. Enriquez, and J. P. Simons, J. Chem. Soc. Faraday Trans. **89**, 1435 (1993).

[24] W. R. Simpson, T. P. Rakitzis, S. A. Kandel, T. Lev-On, and R. N. Zare, J. Phys. Chem. **100**, 7938 (1996).

[25] Y. Matsumi, K. Tonokura, and M. Kawasaki, J. Chem. Phys. **97**, 1065 (1992).

[26] A. J. Orr-Ewing and R. N. Zare, Annu. Rev. Phys. Chem. **45**, 315 (1994).

[27] A. J. Orr-Ewing and R. N. Zare, in *Chemical Dynamics and Kinetics of Small Radicals*, edited by A. Wagner and K. Liu (World Scientific, Singapore, 1995).

[28] N. E. Shafer-Ray, A. J. Orr-Ewing, and R. N. Zare, J. Phys. Chem. **99**, 7591 (1995).

[29] A. J. Orr-Ewing, W. R. Simpson, T. P. Rakitzis, S. A. Kandel, and R. N. Zare, J. Chem. Phys. (submitted).

[30] W. H. Press, B. P. Flannery, S. A. Teukolsky, and W. T. Vetterling, Numerical Recipes (Cambridge University Press, Cambridge, United Kingdom, 1986).

[31] S. S. Parmar and S. W. Benson, J. Am. Chem. Soc. **111**, 57 (1989).

[32] R. D. Levine and R. B. Bernstein, *Molecular Reaction Dynamics and Chemical Reactivity* (Oxford University Press, New York, 1987).

[33] D. F. Varley and P. J. Dagdigian, J. Phys. Chem. **99**, 9843 (1995).

[34] Y.-F. Yen, Z. Wang, B. Xue, and B. Koplitz, J. Phys. Chem. **98**, 4 (1994).

[35] T. N. Truong, D. G. Truhlar, K. K. Baldridge, M. S. Gordon, and R. Steckler, J. Chem. Phys. **90**, 7137 (1989).

[36] K. D. Dobbs and D. A. Dixon, J. Phys. Chem. **98**, 12584 (1994).

[37] D. F. Varley and P. J. Dagdigian, J. Phys. Chem. **100**, 4365 (1995).

[38] X. Wang, M. Ben-Nun, and R. D. Levine, Chem. Phys. **197**, 1 (1995).

[39] I. W. M. Smith, J. Chem. Educ. **59**, 9 (1982).

[40] A. Bottoni and G. Poggi, J. Mol. Struct. (Theochem) **337**, 161 (1995).

[41] J. Park, Y. Lee, J. F. Hershberger, J. M. Hossenlopp, and G. W. Flynn. J. Am. Chem. Soc. **114**, 58 (1992).